Thermal Spray Deposition, Phase Stability and Mechanical Properties of $La_2Zr_2O_7/LaAlO_3$ Coatings

D. Lozano-Mandujano, [1]

C. A. Poblano-Salas, [2]✉

Email carlos.poblano@ciateq.mx

H. Ruiz-Luna, [3]

B. Esparza-Esparza, [1]

A. L. Giraldo-Betancur, [1]

J. M. Alvarado-Orozco, [4]

L. G. Trápaga-Martínez, [1] for this author please include the following text in the affiliation section:

6 On sabatical leave at CIATEQ , [6]

J. Muñoz-Saldaña, [1,5]

[1] Centro de Investigación y de Estudios Avanzados del Instituto Politécnico Nacional Unidad Querétaro, Libramiento Norponiente 2000, Fracc. Real de Juriquilla, C.P. 76230 Querétaro, QRO, Mexico

[2] CIATEQ, Av. Manantiales 23 A Parque Industrial Bernardo Quintana, C.P. 76246 El Marqués, QRO, Mexico

[3] CONACYT – Universidad Autónoma de Zacatecas, Av. Ramón López Velarde 801, C.P. 98000 Zacatecas, Mexico

[4] CIDESI Unidad Querétaro, Av. Pie de la Cuesta 702, Desarrollo San Pablo, C.P. 76130 Querétaro, QRO, Mexico

[5] German Aerospace Center (DLR), Institute of Materials Research, Cologne, Germany

Abstract

This paper deals with the deposition of $La_2Zr_2O_7$ (LZO) and $LaAlO_3$ (LAO) mixtures by air plasma spray (APS). The raw material for thermal spray, single phase LZO and LAO in a 70:30 mol.% ratio mixture was prepared from commercial metallic oxides by high-energy ball milling (HEBM) and high-temperature solid-state reaction. The HEBM synthesis route, followed by a spray-drying process, successfully produced spherical agglomerates with adequate size distribution and powder-flow properties for feeding an APS system. The as-sprayed coating consisted mainly of a crystalline LZO matrix and partially crystalline LAO, which resulted from the high cooling rate experienced by the molten particles as they impact the substrate. The coatings were annealed at 1100 °C to promote recrystallization of the LAO phase. The reduced elastic modulus and hardness, measured by nanoindentation, increased from 124.1 to 174.7 GPa and from 11.3 to 14.4 GPa, respectively, after the annealing treatment. These values are higher than those reported for YSZ coatings; however, the fracture toughness (K_{IC}) of the annealed coating was only 1.04 MPa $m^{0.5}$.

Keywords

mechanical properties
pyrochlores
TBC
thermal spray

Introduction

$La_2Zr_2O_7$ (LZO) is a ceramic compound that crystallizes in the pyrochlore structure and claimed to be promising for applications in thermal barrier coatings (TBC's) due to its outstanding thermal properties, thermal stability up to 2000 °C, low thermal conductivity (1.56 W/m K) and an intrinsic sintering resistance greater than that of standard 7YSZ (Ref 1). However, LZO has a lower thermal expansion coefficient (9×10^{-6} K^{-1}) than YSZ ($10\text{-}11 \times 10^{-6}$ K^{-1}), which can lead to lower quenching stresses but also higher thermal stresses from thermal expansion mismatch during thermal spraying and most importantly, it also suffers from pyrochlore's intrinsic brittleness (Ref 2-5). It has been reported that the K_{IC} values for LZO ceramics depend on their microstructure, having values of

1.40 ± 0.23 MPa m$^{0.5}$ for the microcrystalline form and 1.98 ± 0.07 MPa m$^{0.5}$ when the microstructure is nanocrystalline (Ref 5).

In coatings, LZO have been deposited by air plasma spray (APS) showing excellent thermal stability and thermal shock behavior (Ref 6-8). However, the intrinsic disadvantages of LZO remain, such as low fracture toughness [1.1 ± 0.2 MPa m$^{0.5}$ (Ref 7) and also reported as 1.6 MPa m$^{0.5}$ (Ref 9)]. Furthermore, incompatibility of LZO coatings with the typical thermally grown oxide (TGO) layer, α-Al$_2$O$_3$, limits their application in TBCs. It has been reported that the incompatibility with the TGO can be avoided with a pyrochlore/YSZ double-layer system, which revealed excellent fatigue cyclic testing at temperatures up to 1450 °C (Ref 6, 10). However, even in a double-layer system the problem of intrinsic brittleness of LZO top coats remains unsolved. Mechanical reinforcement of LZO by a second-phase may provide a way to increase its fracture toughness, desirable to remain active at high temperature. Some reports are available related to LZO with second-phase reinforcement. For instance, Li et al. reported values of $K_{IC} = 1.98$ MPa m$^{0.5}$ for a LZO-10-BaTiO$_3$ composite and attributed such increase to BaTiO$_3$ ferroelastic domain switching (Ref 9). Since BaTiO$_3$ is a perovskite with a Curie temperature of 127 °C, associated with a tetragonal-to-cubic phase transformation, above this temperature any effect associated with ferroelastic switching will no longer be active. The fracture toughness of 7YSZ, which is typically used in TBC applications, varies from 1.35 to 2.2 MPa m$^{0.5}$ (Ref 11).

On the other hand, the ZrO$_2$-La$_2$O$_3$-Al$_2$O$_3$ system (Ref 12, 13) shows the existence of a perovskite phase, LaAlO$_3$ (LAO), which is a natural ferroelastic material with a relatively high Curie temperature ($T_c \approx 850$ K), which can coexist in a two-phase region with LZO. LAO has good sintering resistance at high temperatures (Ref 14). Another advantage of LAO is its coefficient of thermal expansion (10×10^{-6} K^{-1}) at temperatures in the range of 500 to 1500 °C, similar to that of 7YSZ (Ref 15). The mechanical properties of LaAlO$_3$ ceramics have been investigated by Liu et al. (Ref 16), reporting values of elastic modulus, Vickers hardness and fracture toughness of 181 ± 31 GPa, 11.1 ± 0.1 GPa and 3.2 ± 0.1 MPa m$^{0.5}$, respectively. As in many materials that undergo a second-order phase transition between the cubic high-temperature phase and the rhombohedral one at lower temperature, ferroelastic twins have been observed at room temperature in LAO (Ref 17). It has been shown elsewhere that domain switching in ferroelastic materials can lead to an increase in toughness as the crack extends (Ref 9, 18, 19). Moreover, no significant volume changes during the cubic-to-rhombohedral phase transition are reported for LAO (Ref 20), making it a potential reinforcing phase in a LZO matrix. Therefore,

investigations of chemical interactions in the ZrO_2-La_2O_3-Al_2O_3 system are worthwhile in determining if the compounds can be effectively used as TBC materials (Ref 13). Hence, the objective of this work is to evaluate the phase stability and mechanical properties of 70:30 mol.% LZO/LAO coatings deposited by APS and to compare such properties with those from well-established ceramics employed in the fabrication of TBC's for gas turbines.

Experimental Procedure

Feedstock Powder Preparation

Lanthanum oxide (99.9%, Alfa Aesar), zirconium oxide (99%, 2% excluding HfO_2, Alfa Aesar), aluminum oxide (99%, Alfa Aesar) and ethyl alcohol (ethanol) were used as raw materials for preparing the coatings. Separately for LZO and LAO powders, stoichiometric amounts of the oxides were weighed and mixed homogeneously with ethanol for 3 h in a planetary mill (Retsch PM 400) at 250 rpm with YSZ balls. Each suspension was completely dried after milling and then calcined for 5 h in a high-temperature furnace (Thermolyne M46100) at 1250 and 1450 °C for LZO and LAO, respectively, in order to promote solid-state reaction that leads to the formation of the desired phases.

The fabricated LZO and LAO powders were mixed in a 70:30 mol.% ratio and milled for 1 h in a planetary mill. A suspension was prepared in deionized water with 70% solids (the powder mixture) and then spray-dried (Triowin SD-1500 Spray Dryer) to produce spherical agglomerates. A spray pressure of 25 KPa, feed rate of 0.5 l/h and inlet temperature of 230 °C were used. The resulting powder was calcined at 1000 °C for 1 h to promote rigidity of the particles. Sieving was performed using a shaking system to separate specific powder size fractions, a particle size of −160 to +20 μm and −100 to +20 μm was used for coatings 1-6 and 7-8, respectively.

Coatings Deposition

APS deposition of the 70:30 powder was carried out using a 9MB plasma spray gun from Sulzer Metco. The powder agglomerates were directly sprayed on grit-blasted AISI 304 stainless steel (SS304) and FeCrAlY (22% Cr, 5.0% Al, 0.1% Y and 0.1% Zr) substrates, with no bond-coat layers or pre-oxidation steps. The FeCrAlY alloy was selected since can simulate the bond-coat layer and also presents comparable oxidation kinetics and thermal expansion coefficient with the bond-coats commonly used in TBC systems (Ref 21). The substrate temperature was maintained at

approximately 300 °C for all experiments. The torch transversal velocity was kept constant at 1 m/s, and the spray distance and current were varied as shown in Table 1.

Table 1

Parameters used for the preparation of coatings

Coating	Spray distance, mm	Current, A
Fixed spray parameters _[The fixed spray parameters included in Table 1 (primary gas flow, secundary gas flow, voltage, carrier gas flow) must be located below the variable spray parameters. Otherwise table 1 is confusing to the reader. I was not able to perform such a change in the row order, please help us modifying Table 1. Please check the original format of the table we already sent to you. Thanks]_		
Primary gas flow, Ar, SLPM	80	
Secondary gas flow, H_2, SLPM	15	
Voltage, V	67	
Carrier gas flow, SLPM	10	
Variable spray parameters		
1	90	515
2	90	568
3	90	620
4	120	515
5	120	568
6	120	620

Powder and Coatings Characterization

Powders and coatings were characterized by x-ray diffraction using a Rigaku Dmax2100 diffractometer with Cu-Kα radiation operated at 30 kV. Transverse cross-sectional coatings were ground using silicon carbide paper (120 to 2400 grid) and subsequently end polished with a commercial colloidal silica suspension (Buehler Mastermet II). Scanning electron micrographs (SEM, Jeol JSM 5800-LV) were employed to assess the morphology and particle-size distribution of the powder, and also the thickness, porosity and microstructure of coatings. The

porosity percentage of the coatings was determined by image analysis from five cross-sectional measurements.

Thermal Properties Measurements

The thermal diffusivity of the specimens was measured using the laser-flash method with a neodymium-glass laser operating at a wavelength of 1064 nm (LINSEIS LFA 1000). Thermal diffusivity values were measured at room temperature, 300, 500 and 1000 °C, all under vacuum.

Mechanical Properties Measurements

A Hysitron Ubi 1 nanoindentation system with a Berkovich diamond tip and variable load (1000 to 9000 μN) was used to determine the hardness and reduced elastic modulus on polished transverse cross sections of the coatings. Indentation imprints in a "load control" mode versus time were carried out. The loading curve was immediately followed by the unloading without 0-s holding time at maximum load. Fracture toughness was determined by employing the indentation crack length method (ICL) using a Vickers microindenter (Shimadzu HMV2000). Crack lengths were measured on SEM micrographs from the indentation imprints.

Results and Discussion

Characterization of the Powder Particles

Before the preparation of the LZO/LAO composites the individual pyrochlore and perovskite phases were separately synthesized. The x-ray diffraction patterns of the LZO and LAO powder after the solid-state synthesis by calcination are shown in Fig. 1. The patterns show no spurious phases according to the JCPDS73-0444 and 31-0022 cards.

Fig. 1

XRD patterns of the (a) pyrochlore, LZO and (b) perovskite, LAO phases synthesized by high-energy ball milling of mixed oxides and solid-state reaction
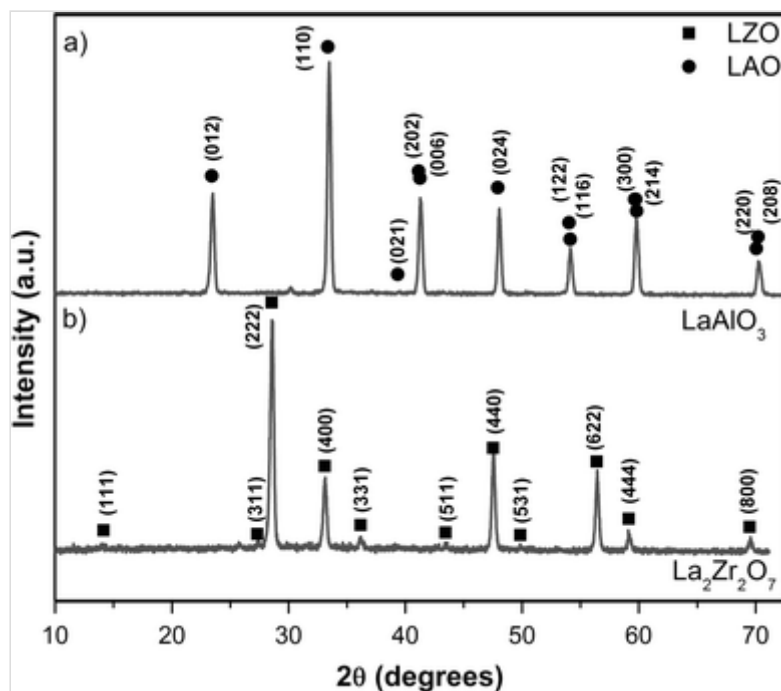
As mentioned before, the LZO and LAO powders were mixed in a 70:30 mol.% ratio, processed by ball milling and spray-dried to prepare the raw material for thermal spray deposition. Figure 2(a) shows typical SEM images of the spray-dried 70:30 LZO/LAO composite powder. The powder was composed of spherical agglomerates with diameters between 20 and 160 μm, with a median size (d_{50}) of 66.6 μm, as obtained from an accumulative distribution (Fig. 2b). The distribution of LAO particles in the spherical agglomerates was also studied. A typical SEM image recorded with a backscattered electron detector was used to identify the distribution of LZO and LAO powder in the agglomerate (Fig. 2c). The agglomerates were formed by equiaxially shaped LZO particles with a size of 1.1 ± 0.3 μm surrounding individual LAO particles with a 4.3 ± 3.1 μm mean size.

Fig. 2

(a) Typical SEM micrograph of the LZO/LAO powder agglomerates after spray drying and calcination, (b) agglomerate size distribution and (c) BSE micrograph used for the identification of LZO and LAO particles in the agglomerates
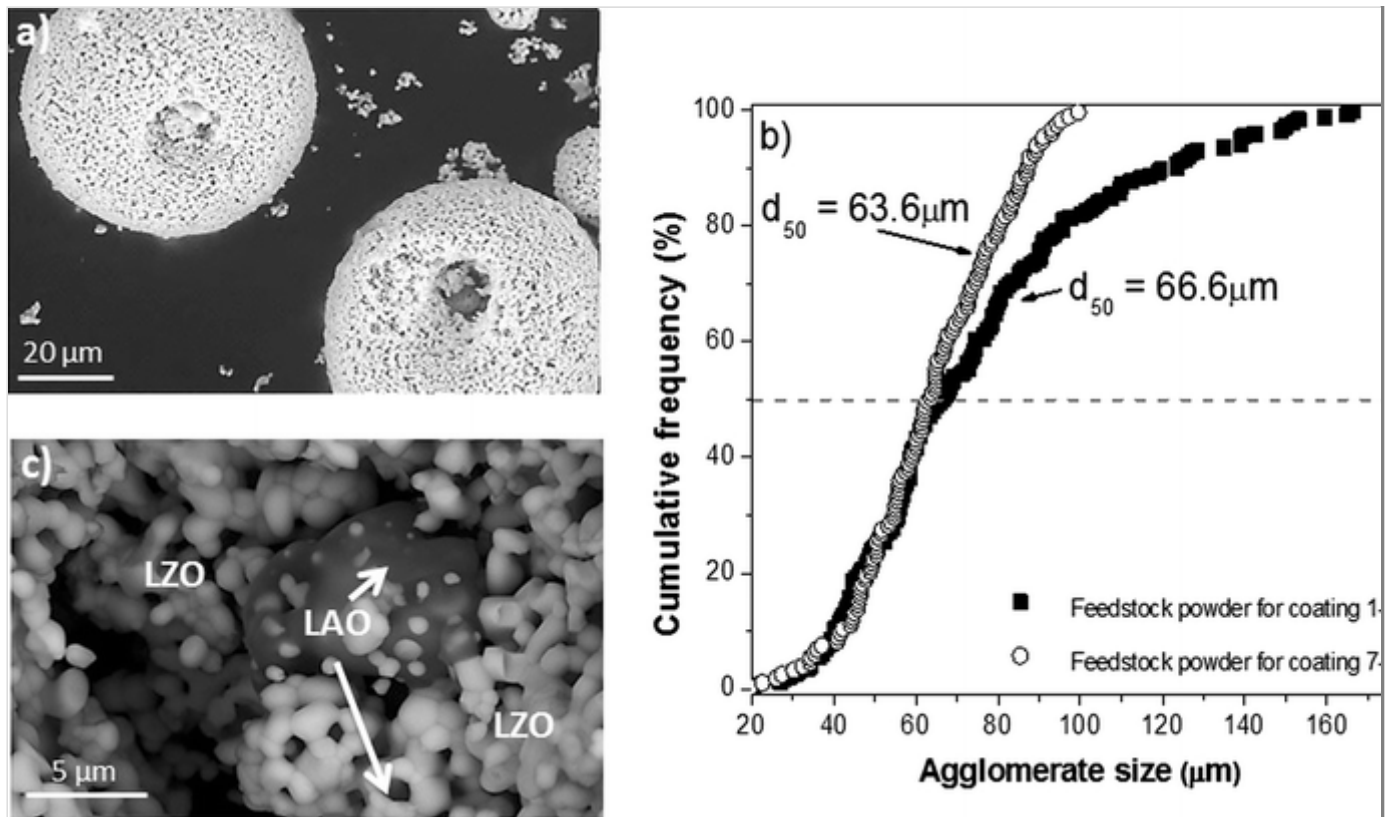
Coatings Characterization

Figure 3 shows a set of SEM micrographs recorded with a backscattering detector from cross sections of the coatings deposited on SS304 substrates. From these micrographs, the effect of both spray distance and current on the quality of the coating (thickness, porosity and adhesion) can be observed. Delamination of the LZO/LAO coatings from the substrate, except of coating 4 which remains attached to the substrate, is noticed. This is probably associated to the thermal stresses generated during cooling as a consequence of the difference between the thermal expansion mismatch between of the stainless steel and the LZO/LAO coatings. The results of thickness and porosity measurements are given in Table 2. In general, an increase in the spray distance from 90 to 120 mm led to a thicker coating for currents of 515 and 568 A. This effect is mitigated and even partially inversed when increasing the current to 620 A (coatings 3 and 6). At a spraying distance of 90 mm, the thickness showed more than a two-fold increase (~220 μm) when the current increased from 515 to 620 A. At 120 mm, the inverse effect is observed, leading to a reduction of the thickness by nearly 30% (~170 μm). It is known that during air plasma spraying, the arc current and the spray distance affects the kinetic and thermal energies of the plasma jet. With an increase in the arc current, the plasma power raised, and higher particle velocity and temperature is attained, which in turn produces higher particle spreading and cohesion of splats causing a decrease in

coatings thickness. Moreover, the use of high arc currents and long spray distances allow a better degree of particle melting, i.e., sufficient flattening on impact, since the dwell time of the particles in the flame increases. Similar results have been previously found by (Ref 22, 23). Contrary to the results of the coatings deposited at 120 mm, at a 90 mm of spray distance, thicker coatings are observed as the current increases. This behavior may be attributed to a combined effect of the spray distance and the gun current. A larger fraction of particles in unmolten state prevail at short spray distances and low current values since the heat input and the residence time of the powder particles in the plasma is insufficient to particle melting. On impact, debonding of the coarser particles and enlarged flattening and fragmentation of the smaller ones may occur. With an increase in the arc current, the adhesion of the particles improves due to the powder melting enhanced and the particles reach the substrate with more adequate in-flight characteristics. Coatings 2 and 5 showed the lowest porosity of the whole set, irrespective of the spray distance; both coatings were sprayed with a current of 568 A. Thus, a current of 568 A leads to good melting of the particles, which is reflected in increased quality of the coatings in terms of porosity.

Fig. 3

Typical cross-sectional SEM micrographs of plasma-sprayed LZO/LAO coatings deposited on SS304 using two spray distances (90 and 120 mm) and three currents (515, 568, and 620 A), conditions 1 to 6 as identified in Table 2
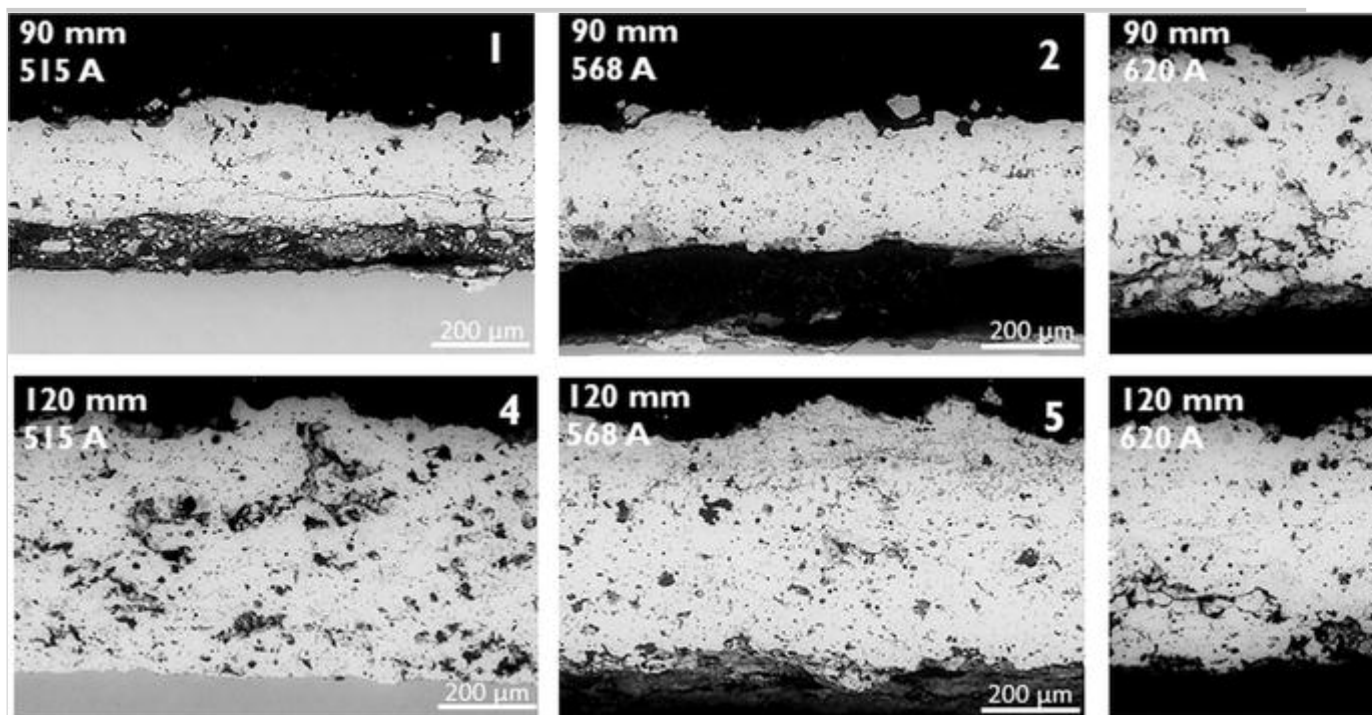
Table 2

Thickness and porosity of "as-sprayed" coatings

Coating	Thickness, μm	Porosity, %
1	191 ± 22	13 ± 3
2	222 ± 17	7 ± 2
3	416 ± 26	13 ± 2
4	569 ± 29	14 ± 1
5	425 ± 38	10 ± 2
6	393 ± 11	12 ± 3

Figure 4 shows XRD patterns of the prepared LZO/LAO coatings in the "as-sprayed" condition and compared with the feedstock powder. All characteristic peaks corresponding to LZO or LAO are present in the diffraction patterns from the feedstock powder. In comparison, a reduction in intensity of the LAO peaks is observed for all conditions of the deposited composite coatings. This is clearly observed in the (012) LAO characteristic peak (~23.4°), since the peak with the highest intensity (110) for the LAO overlapped with the (400) peak from the LZO phase (see Fig. 1). This intensity reduction indicates that a fast crystallization of the LAO phase from molten to solid state at the rapid cooling rates of plasma spraying (~10^6 K s^{-1}) is not occurring. Similar results have been reported by others ceramic systems, including $LaMgAl_{11}O_{19}$, lanthanum magnetoplumbite and mullite (Ref 24-26). On the contrary, the LZO phase remained crystalline due to the fact that pyrochlore structure has higher stability as has been reported by Cao et al. (Ref 27).

Fig. 4

XRD patterns of LZO/LAO as-sprayed coatings using conditions 1 to 6, as detailed in Table 2. The XRD pattern of the feed powder is presented for comparison
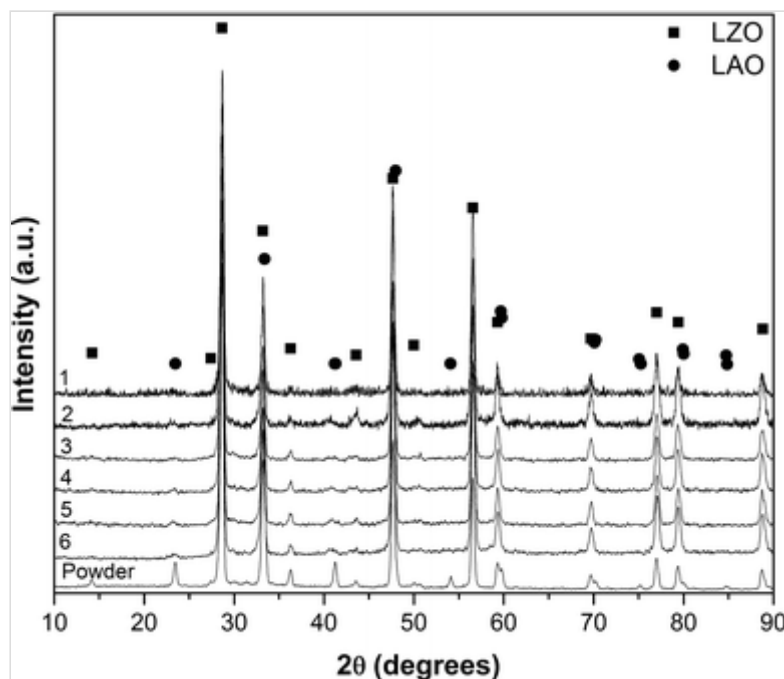
Spallation of the LZO/LAO coatings was observed when the substrate employed was 304 stainless steel (Fig. 3) possibly promoted by thermal mismatch during cooling. For this reason, a new set of LZO/LAO coatings was deposited on FeCrAlY substrates. The spraying parameters for the new set of experiments were chosen based on the previous analysis, maintaining a constant current of 568 A, using both 90 and 120 mm spray distances and narrowing the agglomerate size distribution to a range between 20 and 100 μm, i.e., particles with d_{50} = 63.6 μm. This set of experiments was carried out to evaluate the reproducibility in the preparation of good-quality coatings in terms of porosity and adhesion and avoid coating spallation or delamination due to thermal mismatch between the ceramic coating and the substrate.

Figure 5 shows an analysis of the cross sections of the second set of LZO/LAO coatings deposited on FeCrAlY substrates at 90 and 120 mm spray distance, respectively. The SEM micrographs show differences in coating porosity and thickness arising from the difference in spraying distance. The thickness of the coatings sprayed at 90 mm was 173 ± 12 μm, whereas for samples sprayed at 120 mm an average thickness of 190 ± 15 μm was measured. The reduction in thickness may be attributed to the narrower agglomerate size distribution used in the second set of experiments, as the number of passes was the same for both spraying distances. The average porosity was 9 ± 2% and 11 ± 2% for coatings sprayed at 90 and 120 mm, respectively. These values are slightly larger than, but statistically equivalent, to the values for the coatings deposited on SS304. Irrespective of the spray distance employed, all coatings showed a lamellar

microstructure having a combination of both fully melted splat lamellae and unmelted regions within splats. This type of microstructure has been previously reported for coatings deposited using nanostructured Al_2O_3-13wt.%TiO_2 powders (Ref 28, 29) and is claimed to result from a short residence time of the agglomerate powder inside the plasma jet (approximately 0.1 ms) which in turn leads to incomplete melting of the particles (Ref 30). The melting extent of a particle in the plasma jet depends on its size, thermal conductivity, latent heat and trajectory (Ref 30). In our case, the unmelted regions found in the coatings are not linked to a preferred phase. Finally, no traces of spallation were observed in the coatings deposited on FeCrAlY.

Fig. 5

Typical cross-sectional SEM micrographs recorded at increasing magnifications for plasma-sprayed LZO/LAO coatings deposited on FeCrAlY substrate at spray distances of (a-c) 90 and (d-f) 120 mm
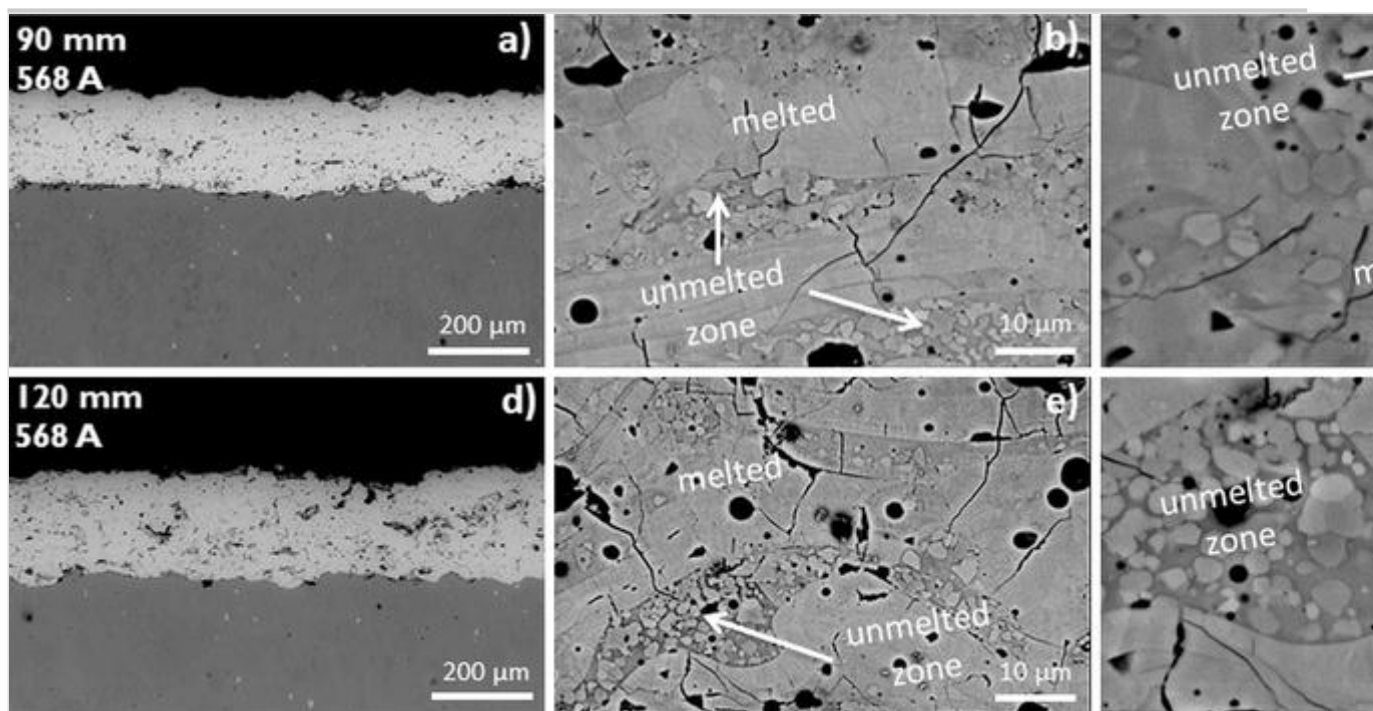

Figure 6 shows typical XRD patterns of the LZO/LAO coating sprayed at 90 mm on FeCrAlY substrates in the "as-sprayed" condition and after a heat treatment. The as-sprayed coating (Fig. 6a) showed identical behavior compared to the first set of coatings sprayed on SS304 substrates, this is, the pyrochlore and perovskite phases corresponding to LZO and LAO, respectively, were detected and an important reduction of intensity in peak (012) for the LAO phase was observed. Instead, both phases LAO and LZO were identified for the coating heat treated at 1100 °C for

4 h. During the heat treatment, a complete recrystallization of the LAO phase occurred and an increase in the relative intensities of different LAO peaks ~~is~~ was observed (2θ ~23.4, 41.3 and 54.1°).

Fig. 6

XRD patterns of LZO/LAO deposited on FeCrAlY at 90 mm, (a) "as sprayed" and (b) after subsequent heat treating at 1100 °C for 4 h. The pattern of the feed powder is included for comparison purposes
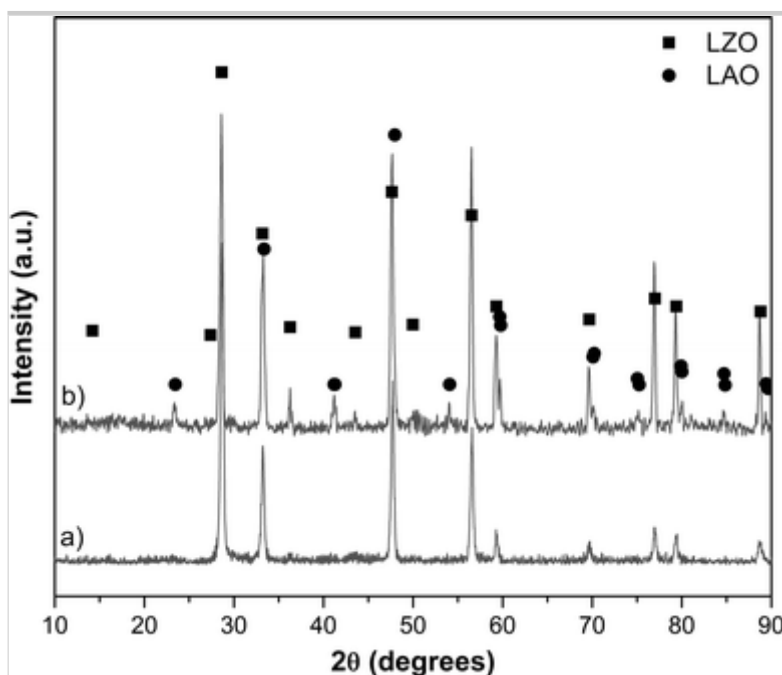

Thermal Properties

The primary function of a TBC is thermal insulation. Figure 7 shows the thermal diffusivity of a LZO/LAO coating processed in this work; the diffusivity of a LZO/LAO bulk composite, pure LZO powder, pure LAO powder and an YSZ coating are also included for comparative purposes. The thermal diffusivity of all samples decreased with increasing temperature, as expected. For instance, the bulk LZO/LAO ceramic decreased from 0.0105 cm^2 s^{-1} at 25 °C to 0.0062 cm^2 s^{-1} at 800 °C, whereas for the LZO/LAO coating, having an 11% porosity, the thermal diffusivity decreased from 0.0080 to 0.0045 cm^2 s^{-1} over the same temperature range. The results suggest that there is an increase in thermal diffusivity with temperature for the LZO/LAO bulk sample at temperatures above 600 °C, but more work has to be done to confirm this effect.

Fig. 7

Thermal diffusivity of LZO, LAO and 70:30 LZO/LAO ceramics, 70:30 LZO/LAO and YSZ coatings
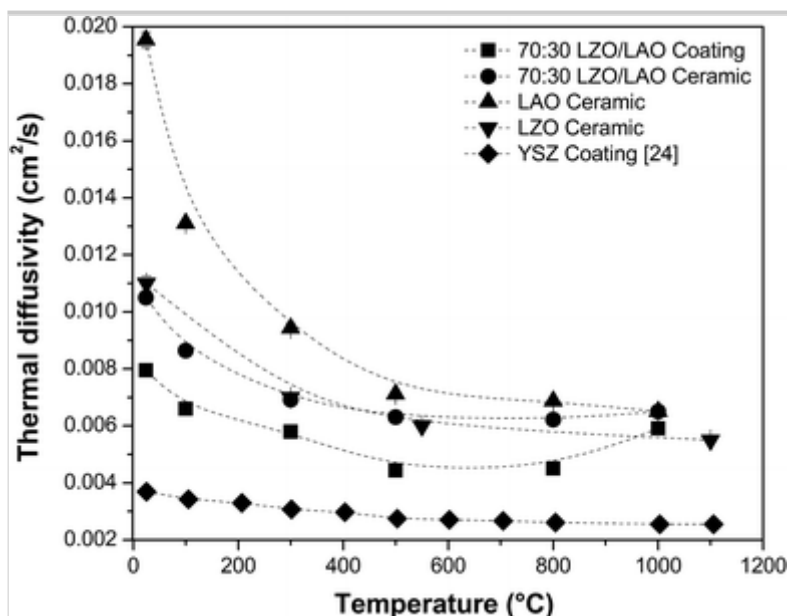
The lower thermal diffusivity values of the LZO/LAO coating compared to the bulk specimen are attributed to its porosity content and presence of defects, which are higher compared to the bulk sample. It has been reported that the thermophysical characteristics of thermal spray coatings, including the thermal diffusivity, are dependent on the porosity percentage, defects such as cracks and voids, phase composition and crystal grains size (Ref 31). For high-temperature measurements (~1000 °C), the increase observed in thermal diffusivity is probably related to the sintering effect and recrystallization, which is consistent with the XRD findings for the heat-treated sample. The diffusivity values of the coating are lower than those of each single phase (LZO and LAO) and the bulk specimen, but still higher than those reported for the YSZ coating (Ref 32).

Mechanical Properties

The mechanical properties of the ceramic layer play a very important role in TBC systems. In this work, employing nanoindentation curves, the indentation hardness (H) and elastic modulus (E_r) of the LZO/LAO coatings were determined using the Oliver Pharr method (Ref 33). The average values of H and E_r were 11.3 ± 2.4 and 124.1 ± 22.3 GPa, respectively, for the coating sprayed at 90 mm, and 14.0 ± 1.0 and 147.7 ± 13.2 GPa for the coating sprayed at 120 mm. Hardness of the coating was found to increase with the spray distance. At larger spray distances (120 mm) the powder particles attain a longer residence time in contact with the plasma jet,

increasing their temperature and improving their melting condition which in turn increases the coating hardness. Similar results have been found for APS coatings where short distances are insufficient for particle melting, yielding to a coating with low hardness (Ref 22, 23). In these works, it has been also reported that at longer spray distances the in-flight particle temperature is high enough for producing better particle melting and therefore increased hardness, bond strength and deposition efficiency.

On the processing of nanostructured zirconia coatings by plasma spray it has been reported that having melted and unmelted zones in the microstructure produce a bimodal distribution of the mechanical properties (Ref 34). Figure 8 compares the Weibull probability function plots for nanoindentation hardness and reduced elastic modulus for the coatings sprayed at 90 and 120 mm on FeCrAlY substrates. From these curves it can be seen that both hardness and elastic modulus data show scattering, a typical behavior of the heterogeneous microstructure of as-sprayed coatings. Deviations from a straight line in the Weibull fit are clearly observed. Such deviations result in large variations of the Weibull modulus "m" coefficient (the slope of Weibull fit plot). This parameter is a measure of the standard deviation and also indicates the reliability of the experimental data. The region of the Weibull plot at higher hardness and elastic modulus values reflects the mechanical behavior of fully melted splats, whereas the region at lower hardness values is representative of zones consisting of unmelted and porous particles embedded in the coating microstructure. Figure 8 also shows the mechanical behavior of the LZO/LAO coating sprayed at 90 mm with and without a heat treatment. The analysis showed that the values of hardness and reduced elastic modulus are higher for the heat-treated coating (H = 16.7 GPa and E_r = 202.8 GPa) than for the coating in its as-sprayed condition (H = 11.3 ± 2.4 GPa and E_r = 124.1 ± 22.3 GPa). This mechanical behavior is attributed to the sintering of the coating during the heat treatment which reduces the porosity content and enhances splats cohesion resulting in superior coating hardness and elastic modulus (Ref 31). Deviation from a straight line was greatly reduced for the heat-treated coating.

Fig. 8

Weibull plots of nanoindentation results for (a) hardness and (b) reduced elastic modulus for the 70:30 LZO/LAO coatings deposited on FeCrAlY and for the 90 mm sample after heat treating

(a)

(b)
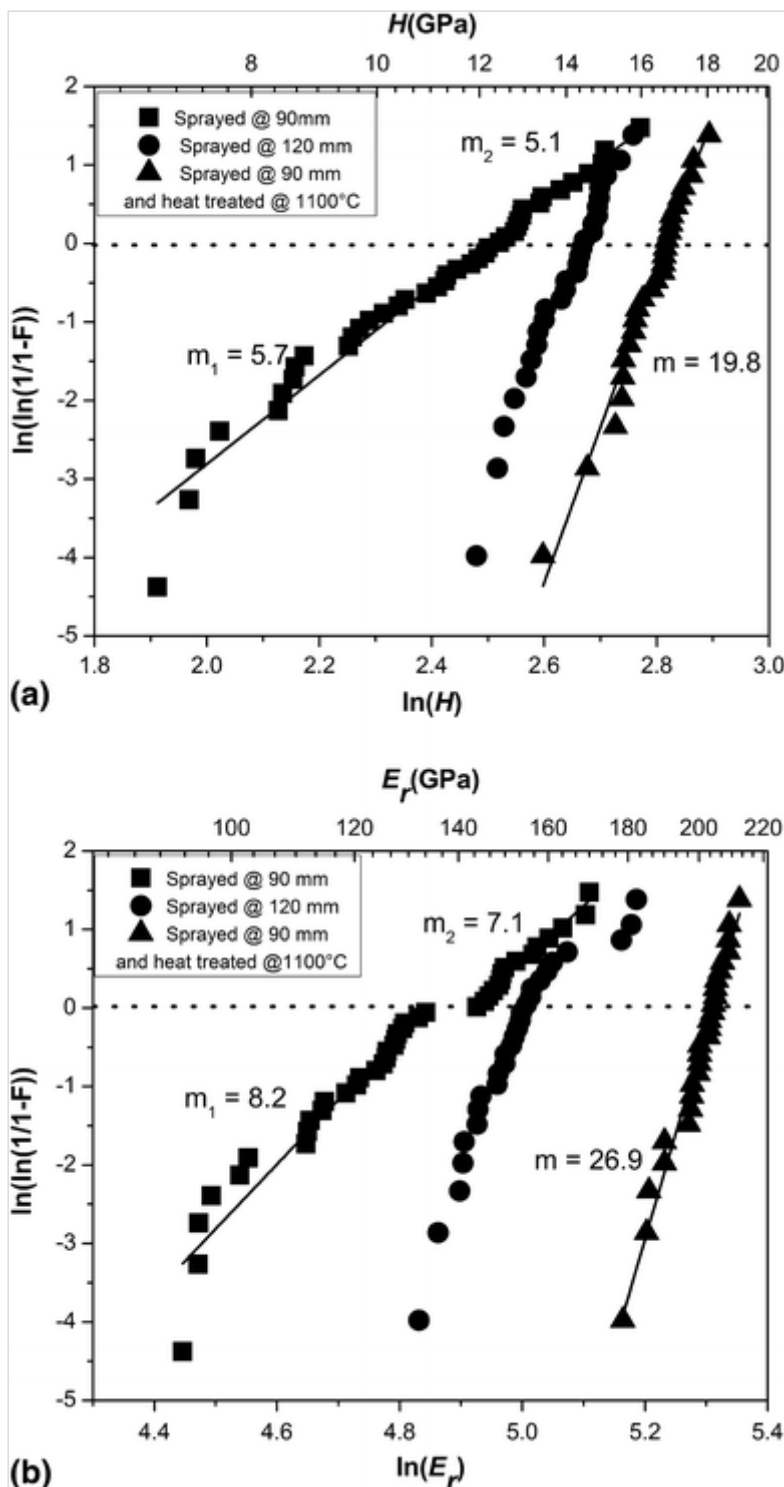
Fracture toughness of the heat-treated LZO/LAO coating was measured by following the ICL method. Measurements were not possible in the "as-sprayed" coatings, because of their brittle behavior (excessive cracking and spallation) during the microindentation testing. The fracture toughness of heat-treated 70:30 LZO/ LAO coating measured in this work was 1.04 MPa $m^{0.5}$, which was still low compared to values reported for plasma-sprayed LZO (1.4 MPa $m^{0.5}$) and YSZ (1.8 MPa $m^{0.5}$) coatings (Ref 35). Since toughening is not occurring in heat-treated LZO/LAO APS coatings, it remains unclear whether the ferroelastic behavior is

inactive due to the small grain size, or if it merely has little impact on fracture toughness.

Conclusions

Synthesis of $La_2Zr_2O_7$ and $LaAlO_3$ powder mixtures with suitable characteristics for feeding an APS system was produced by HEBM, high-temperature solid-state reaction and spray drying, thus providing a potential alternative for large-scale production of rare-earth feedstock for deposition by air plasma spraying. A 70:30 mol.% ratio LZO/LAO coating was also successfully obtained by air plasma spray without significant deviation from the target composition. The high cooling rate that the molten powder particles underwent when impacting the substrate during the deposition process resulted in a blend of crystalline phases and a highly brittle coating, a condition that is slightly improved by an annealing heat treatment. Further work needs to be performed to reduce the quenching rate that may diminish or prevent the deposition of $LaAlO_3$ in a glassy state. Although the fracture toughness of LZO/LAO coatings was improved as the crystalline fraction of $LaAlO_3$ increases with heat treatment, the values are still low when compared with those of ceramics employed traditionally as TBCs.

Acknowledgments

References

1. R. Vaßen, M.O. Jarligo, T. Steinke, D.E. Mack, and D. Stöver, Overview on Advanced Thermal Barrier Coatings, *Surf. Coat. Technol.*, 2010, **205**, p 938-942

2. C.G. Levi, Emerging Materials and Processes for Thermal Barrier Systems, *Curr. Opin. Solid State Mater.*, 2004, **8**, p 77-91

3. X.Q. Cao, R. Vassen, and D. Stöver, Ceramic Materials for Thermal Barrier Coatings, *J. Eur. Ceram. Soc.*, 2004, **24**, p 1-10

4. H. Lehmann, D. Pitzer, G. Pracht, R. Vassen, and D. Stöver, Thermal Conductivity and Thermal Expansion Coefficients of the Lanthanum Rare-Earth-Element Zirconate System, *J. Am. Ceram. Soc.*, 2003, **86**, p 1338-1344

5. J.Y. Li, H. Dai, Q. Li, X.H. Zhong, and X.Q. Cao, Improvement of Fracture Toughness Lanthanum Zirconate, *Cailiao Gongcheng*, 2006, **5**, 51-56, 62

6. L. Wang, Y. Wang, X.G. Sun, J.Q. He, Z.Y. Pan, and C.H. Wang, Thermal Shock Behavior of 8YSZ and Double-Ceramic-Layer $La_2Zr_2O_7$/8YSZ Thermal Barrier Coatings Fabricated by Atmospheric Plasma Spraying, *Ceram. Int.*, 2012, **38**, p 3595-3606

7. R. Vassen, X. Cao, F. Tietz, D. Basu, and D. Stöver, Zirconates as New Materials for Thermal Barrier Coatings, *J. Am. Ceram. Soc.*, 2000, **83**, p 2023-2028

8. X.Q. Cao, R. Vassen, W. Jungen, S. Schwartz, F. Tietz, and D. Stöver, Thermal Stability of Lanthanum Zirconate Plasma-Sprayed Coating, *J. Am. Ceram. Soc.*, 2001, **84**, p 2086-2090

9. J.Y. Li, H. Dai, X.H. Zhong, Y.F. Zhang, X.F. Ma, J. Meng, and X.Q. Cao, Lanthanum Zirconate Ceramic Toughened by $BaTiO_3$ Secondary Phase, *J. Alloys Compd.*, 2008, **452**, p 406-409

10. R. Vaßen, F. Traeger, and D. Stöver, New Thermal Barrier Coatings Based on Pyrochlore/YSZ Double-Layer Systems, *Int. J. Appl. Ceram. Technol.*, 2004, **1**, p 351-361

11. G. Dwivedi, V. Viswanathan, S. Sampath, A. Shyam, and E. Lara-Curzio, Fracture Toughness of Plasma-Sprayed Thermal Barrier Ceramics: Influence of Processing, Microstructure, and Thermal Aging, *J. Am. Ceram. Soc.*, 2014, **97**, p 2736-2744

12. O. Fabrichnaya, S. Lakiza, Ch. Wang, M. Zinkevich, and F. Aldinger, Assessment of Thermodynamic Functions in the ZrO_2-La_2O_3-Al_2O_3 System, *J. Alloys Compd.*, 2008, **453**, p 271-281

13. O. Fabrichnaya, G. Savinykh, and G. Schreiber, Phase Relations in the ZrO_2-La_2O_3-Y_2O_3-Al_2O_3 System: Experimental Studies and Phase Modeling, *J. Eur. Ceram. Soc.*, 2013, **33**, p 37-49

14. P.K. Sahua, S.K. Behera, S.K. Pratihar, and S. Bhattacharyya, Low Temperature Synthesis of Microwave Dielectric $LaAlO_3$ Nanoparticles: Effect of Chloride on Phase Evolution and Morphology, *Ceram. Int.*, 2004, **30**, p 1231-1235

15. B.C. Chakoumakos, D.G. Schlom, M. Urbanik, and J. Luine, Thermal Expansion of LaAlO3 and (La, Sr)(Al, Ta)O3, Substrate Materials for Superconducting Thin-Film Device Applications, *J. Appl. Phys.*, 1998, **83**, p 1979-1982

16. X.Q. Liu and X.M. Chen, Dielectric and Mechanical Characteristics of Lanthanum Aluminate Ceramics with Strontium Niobate Addition, *J. Eur. Ceram. Soc.*, 2004, **24**, p 1999-2004

17. P.D. Tall, C. Coupeau, and J. Rabier, Indentation-Induced Twinning in $LaAlO_3$ Single Crystals: An Atomic Force Microscopy Study, *Scr. Mater.*, 2003, **49**, p 903-908

18. C. Mercer, J.R. Williams, D.R. Clarke, and A.G. Evans, On a Ferroelastic Mechanism Governing the Toughness of Metastable Tetragonal-Prime (t′) Yttria-Stabilized Zirconia, *Proc. R. Soc. A*, 2007, **463**, p 1393-1408

19. T.A. Schaedler, R.M. Leckie, S. Krämer, A.G. Evan, and C.G. Levi, Toughening of Nontransformable t′-YSZ by Addition of Titania, *J. Am. Ceram. Soc.*, 2007, **90**, p 3896-3901

20. C.H. Kim, J.W. Jang, S.Y. Cho, I.T. Kim, and K.S. Hong, Ferroelastic Twins in $LaAlO_3$ Polycrystal, *Phys. B*, 1999, **262**, p 438-443

21. M. Schweda, T. Beck, M. Offermann, and L. Singheiser, Thermographic Analysis and Modelling of the Delamination Crack Growth in a Thermal Barrier Coating on Fecralloy, *Surf. Coat. Technol.*, 2013, **217**, p 124-128

22. C.S. Ramachandran, V. Balasubramanian, and P.V. Ananthapadmanabhan, Multiobjective Optimization of Atmospheric Plasma Spray Process Parameters

to Deposit Yttria-Stabilized Zirconia Coatings Using Response Surface Methodology, *J. Therm. Spray Technol.*, 2011, **20**, p 590-607

23.   S. Datta, D.K. Pratihar, and P.P. Bandyopadhyay, Modeling of Plasma Spray Coating Process Using Statistical Regression Analysis, *Int. J. Adv. Manuf. Technol.*, 2013, **65**, p 967-980

24.   X.Q. Cao, Y.F. Zhang, J.F. Zhang, X.H. Zhong, Y. Wang, H.M. Ma, Z.H. Xu, L.M. He, and F. Lu, Failure of the Plasma-Sprayed Coating of Lanthanum Hexaluminate, *J. Eur. Ceram. Soc.*, 2008, **28**, p 1979-1986

25.   C. Friedrich, R. Gadow, and T. Schirmer, Lanthanum Hexaaluminate—a New Material for Atmospheric Plasma Spraying of Advanced Thermal Barrier Coatings, *J. Therm. Spray. Technol.*, 2001, **10**, p 592-598

26.   L.L. Huang, H.M. Meng, and J. Tang, Crystallization Behavior Of Plasma-Sprayed Lanthanide Magnesium Hexaaluminate Coatings, *Int. J. Miner. Metall. Mater.*, 2014, **21**, p 1247-1253

27.   X.Q. Cao, R. Vassen, W. Jungen, S. Schwartz, F. Tietz, and D. Stöver, Thermal Stability of Lanthanum Zirconate Plasma-Sprayed Coating, *J. Am. Ceram. Soc.*, 2001, **84**, p 2086-2090

28.   M. Gell, E.H. Jordan, Y.H. Sohn, D. Goberman, L. Shaw, and T.D. Xiao, Development and Implementation of Plasma Sprayed Nanostructured Ceramic Coatings, *Surf. Coat. Technol.*, 2001, **146-147**, p 48-54

29.   D. Goberman, Y.H. Sohn, L. Shaw, E. Jordan, and M. Gell, Microstructure Development of Al_2O_3-13 wt.% TiO_2 Plasma Sprayed Coatings Derived from Nanocrystalline Powder, *Acta Mater.*, 2002, **50**, p 1141-1152

30.   H.B. Xiong, L.L. Zheng, L. Li, and A. Vaidya, Melting and Oxidation Behavior of In-Flight Particles in Plasma Spray Process, *Int. J. Heat Mass Transf.*, 2005, **48**, p 5121-5133

31.   L. Pawlowski, *The Science and Engineering of Thermal Spray Coatings*, 2nd ed., Wiley, New York, 2008

32. R.E. Taylor, X. Wang, and X. Xu, Thermophysical Properties of thermal Barrier Coatings, *Surf. Coat. Technol.*, 1999, **120-121**, p 89-95

33. W.C. Oliver and G.M. Pharr, An Improved Technique for Determining Hardness and Elastic Modulus Using Load and Displacement Sensing Indentation Experiments, *J. Mater. Res.*, 1992, **7**, p 1564-1583

34. G. Di Girolamo, F. Marra, C. Blasi, E. Serra, and T. Valente, Microstructure, Mechanical Properties and Thermal Shock Resistance of Plasma Sprayed Nanostructured Zirconia Coatings, *Ceram. Int.*, 2011, **37**, p 2711-2717

35. C.S. Ramachandran, V. Balasubramanian, and P.V. Ananthapadmanabhan, On the Cyclic Hot Corrosion Behaviour of Atmospheric Plasma Sprayed Lanthanum Zirconate Based Coatings in Contact with a Mixture of Sodium Sulphate and Vanadate Salts: A Comparison with the Traditional YSZ Duplex and NiCrAlY Coated Samples, *Vacuum*, 2013, **97**, p 81-95